Tracing Saharan dust to the Eastern Mediterranean: Integrating mineralogical and isotopic proxies with atmospheric trajectory modelling

S. Bitzan[1], C.L. Blanchet[2], S. Pichat[3,4], G. Christidis[5], K. Schepanski[6,7], F. Kirsten[1,8]

[1]*Institute of Geographical Science, Department of Earth Sciences, Freie Universität Berlin, Berlin, Germany*
[2]*GFZ Helmholtz Centre for Geosciences, Section 4.6 Geomorphology, Potsdam, Germany*
[3]*Univ Lyon, ENSL, UCBL, UJM, CNRS, LGL-TPE, Lyon, France*
[4]*Max Planck Institute for Chemistry, Mainz, Germany*
[5]*School of Mineral Resources Engineering, Technical University of Crete, Chania, Greece*
[6]*Institute of Meteorology, Department of Earth Sciences, Freie Universität Berlin, Germany*
[7]*Leibniz Institute for Tropospheric Research (TROPOS), Modelling of Atmospheric Processes, Leipzig, Germany*
[8]*Institute of Geography, Department of Computational Landscape Ecology, Technische Universität Dresden, Dresden, Germany*

Navigation

1. Fingerprinting of dust samples

1.1 Research Area and Sampling

1.2 Sample Introduction

1.3 Mineralogical Composition

1.4 Grain-Size Distribution

1.5 Isotopic Composition

1.6 Potential Source Areas

1.7 Main Findings from Fingerprinting

2. Trajectory Analyses

2.1 Definition of Dust Days

2.2 Trajectories and Cluster Analysis

2.3 Regression Analysus

2.4 Composite Plots

3. Conclusion



1.1 Research Area & Sampling

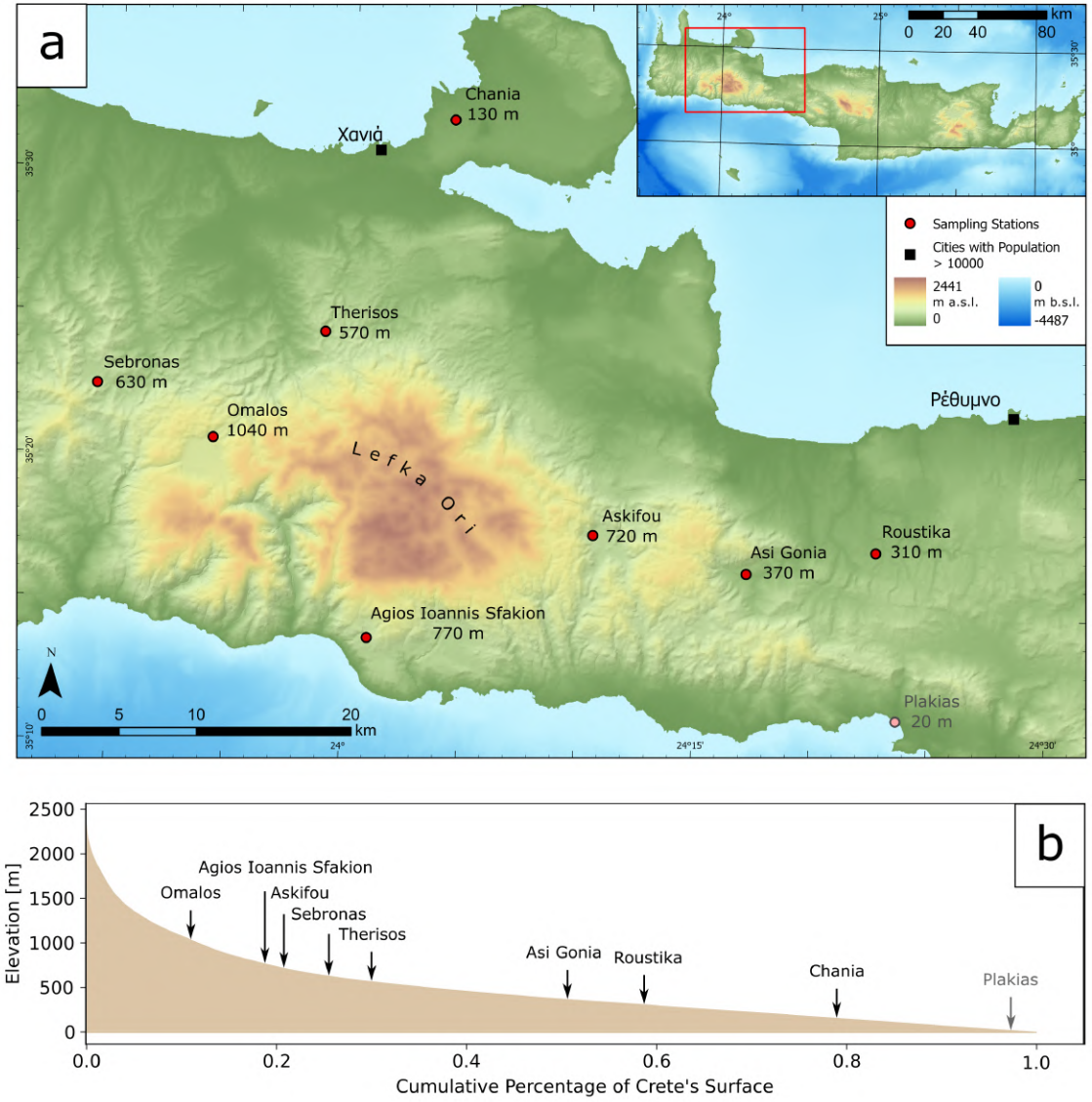


Figure 1:
a - Study area with locations of sampling Stations;
b - Location of sampling stations in hypsogramm of Crete
(Bitzan et al. 2025a)

In Section 1, only the deposition samples of the marble sampler were used

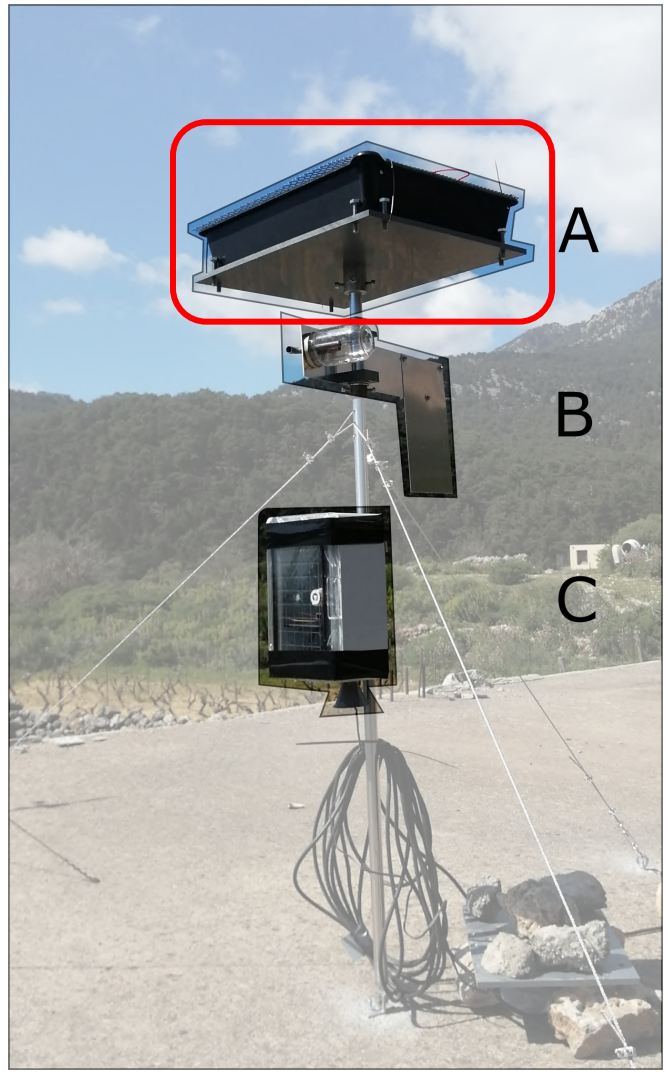
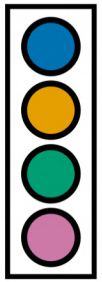


Figure 2: Sampling station in Agios Ioannis Sfakion.
A - Marble Sampler;
B - MWAC;
C - OPC

1.2 Sample Introduction



Mineralogical Composition
Grain-size Distribution
Sr-Nd-Isotopy
Pb-Isotopy

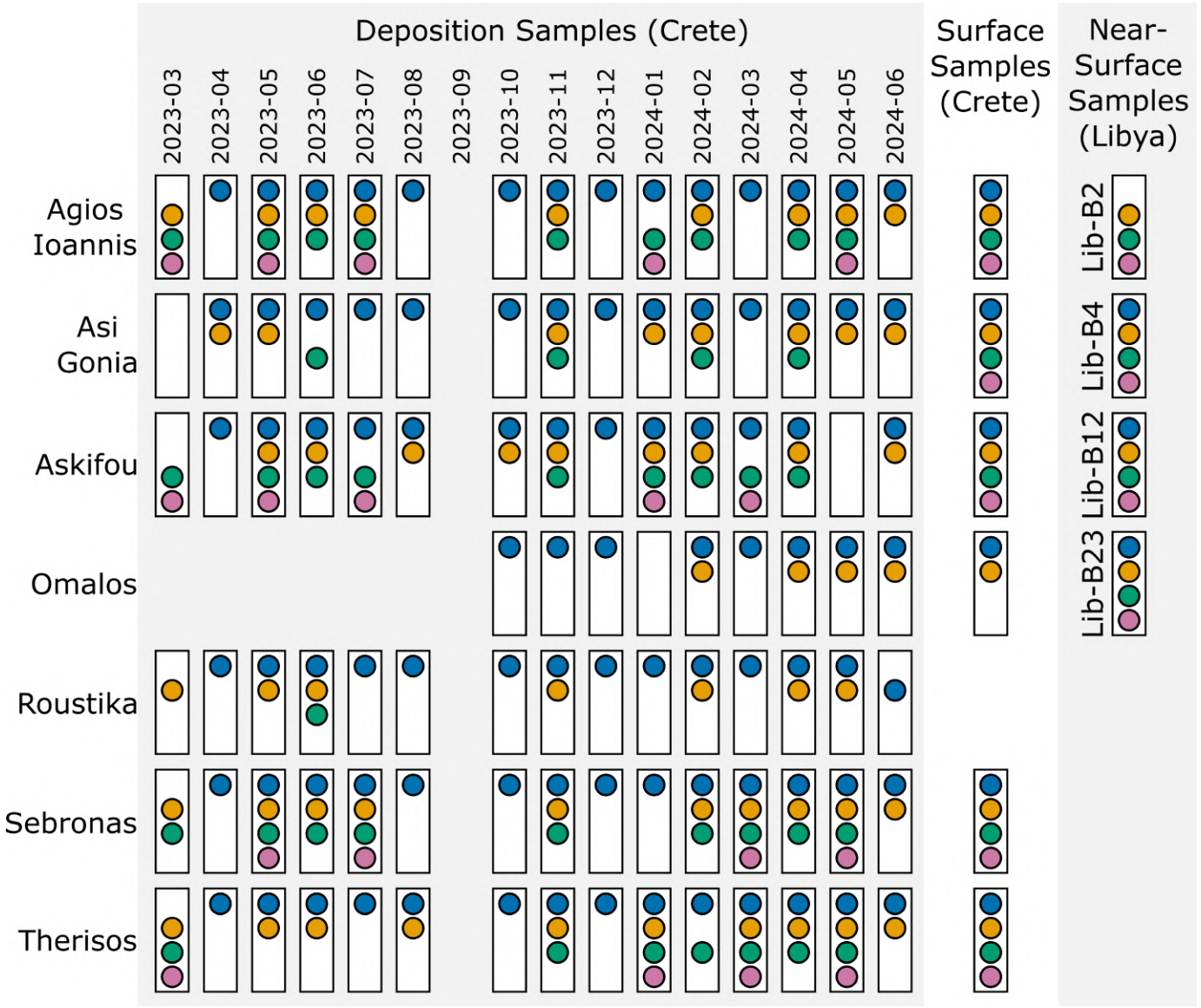


Figure 3: Overview of the deposition samples used and the analyses performed: blue – mineralogy; orange – grain size; green – Nd-Sr-isotopy; violet – Pb-isotopy (Bitzan et al. 2025b)

1.3 Mineralogical Composition

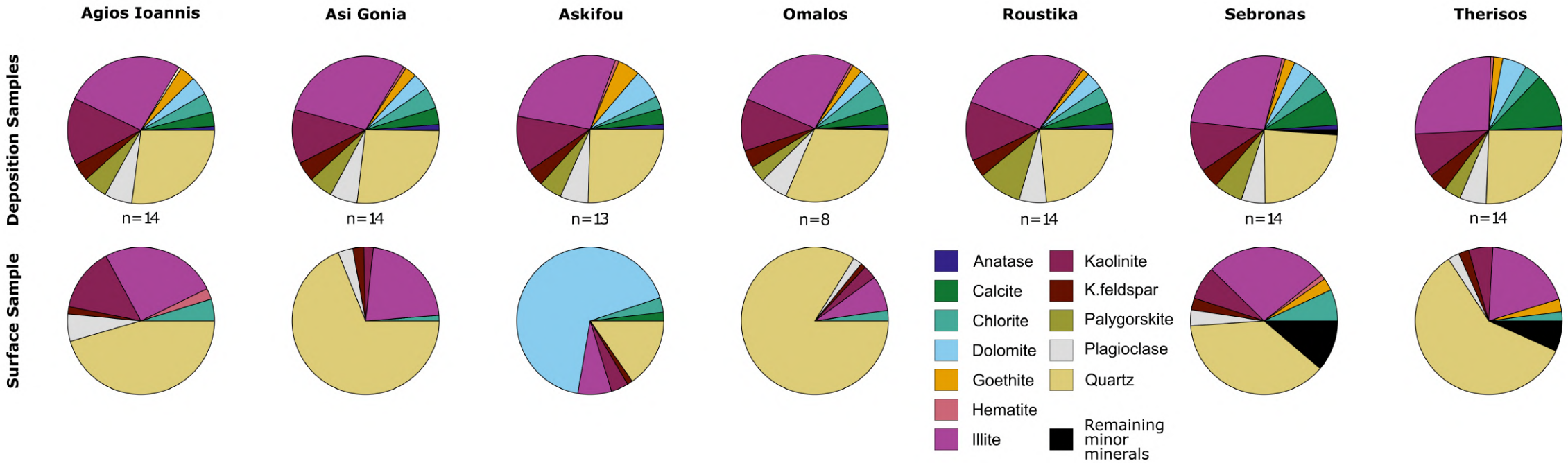


Figure 4: Mineralogical composition of samples; top – median of all deposition samples from each station; bottom – composition of surface sample from the respective station (Bitzan et al. unpublished data - under review)

- Similar compositions of deposition samples at different stations
- Varying compositions of surface samples at different stations

1.3 Mineralogical Composition

- Varying contents and ranges over time
- Similar contents and ranges at different stations

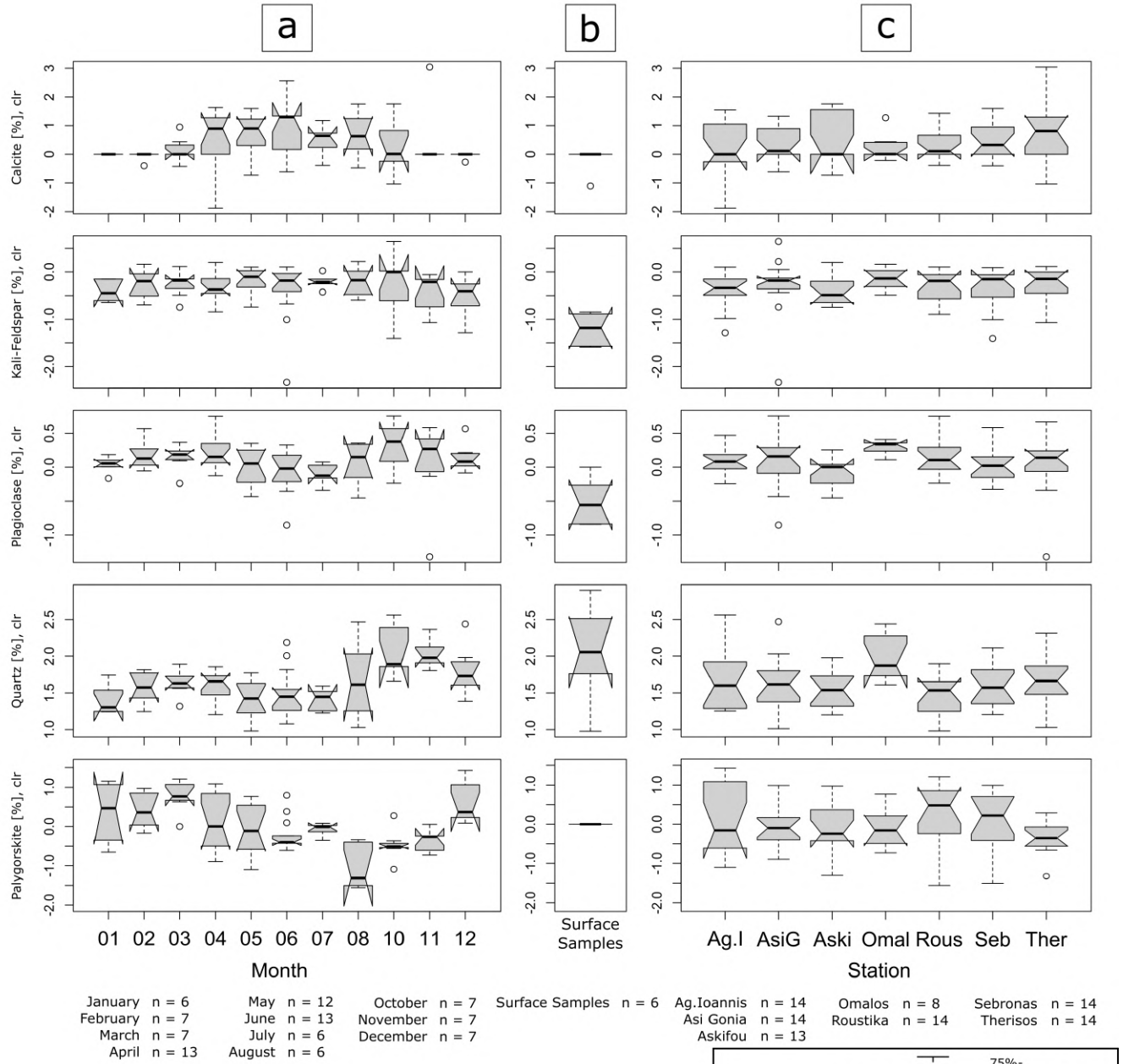
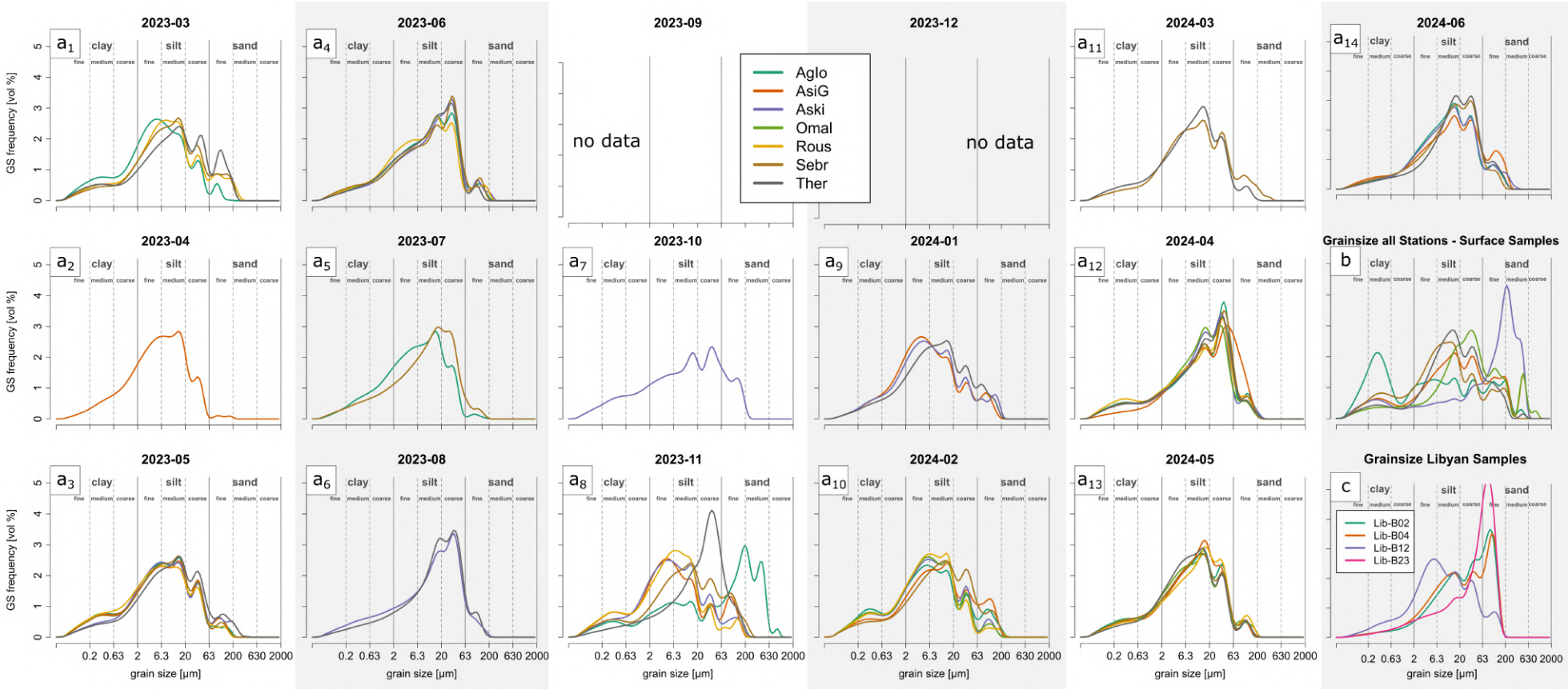


Figure 5: Boxplots of selected clr-transformed mineral contents from deposition samples of all stations grouped by (a) months and grouped by (c) locations. (b) mineral contents of surface samples taken near the stations (Bitzan et al. unpublished data - under review)

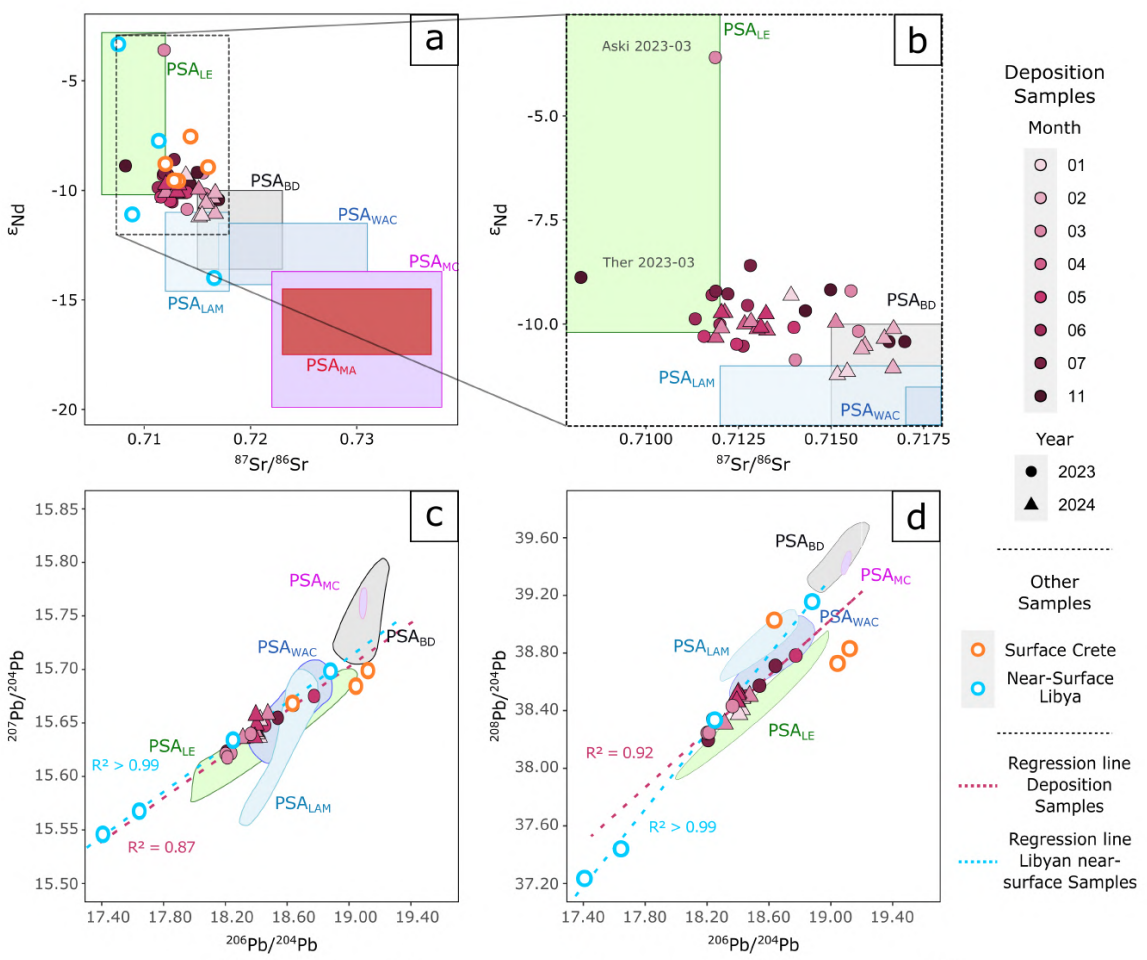
1.4 Grainsize Distribution



- Similar distributions and means in monthly grouped deposition samples
- Varying distributions and ranges of surface samples

Figure 6: a_1–a_{14} – Grain size distribution of deposition samples from all stations grouped by months (absence of curve or empty plots means that the small sample quantities did not allow for grain size measurements); b – Grain size distribution of surface samples; c – Grain size distribution of Libyan near-surface aerosol samples (Bitzan et al. unpublished data - under review)

1.5 Isotopic Composition (Sr, Nd, Pb)



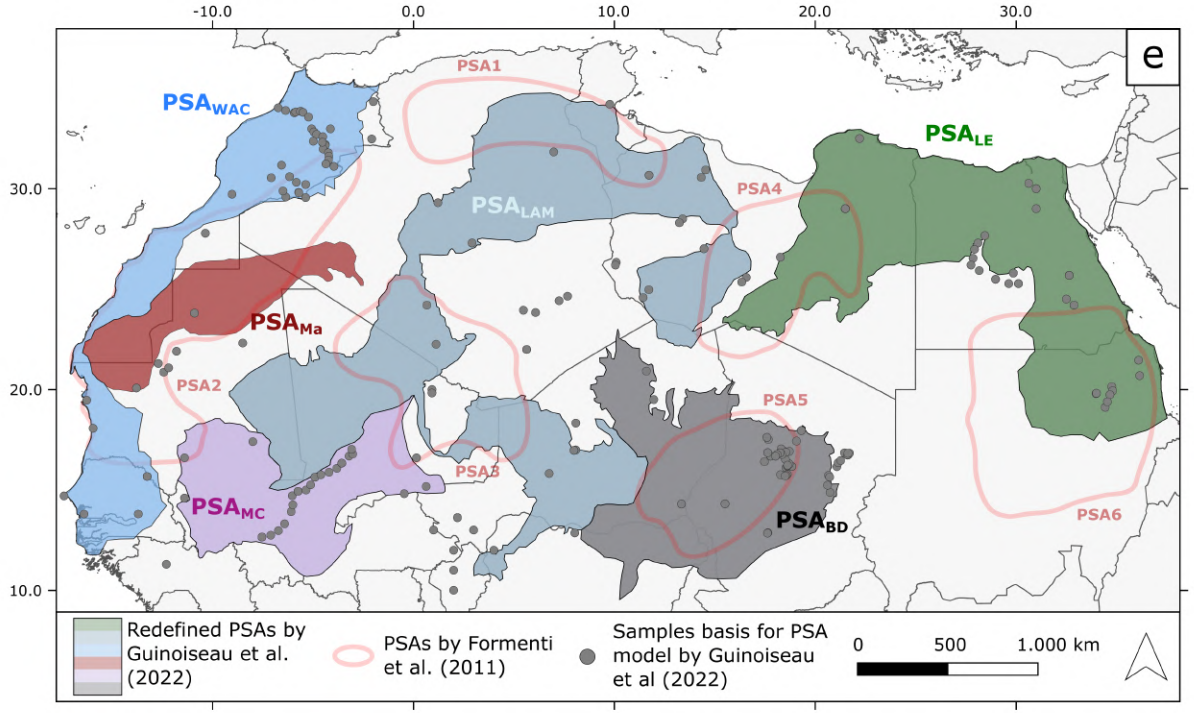


Figure 7: a – Sr-Nd-isotope ratios of deposition samples from Crete grouped according to sampling months including surface samples from Crete and near-surface samples from Libya; b – Zoom on Sr-Nd-isotope ratios of Cretan deposition samples; c, d – $^{207}Pb/^{204}Pb$ vs. $^{206}Pb/^{204}Pb$ and $^{208}Pb/^{204}Pb$ vs. $^{206}Pb/^{204}Pb$ ratios of Cretan deposition samples grouped according to sampling months (Bitzan et al. unpublished data - under review); e - Potential source areas of North African dust based on the extension of geological provinces

The combination of strontium, neodymium, and lead isotopes shows the strongest correlation between the samples and PSA_{LAM}, PSA_{LE}, and the areas in between.

1.6 Potential Source Areas

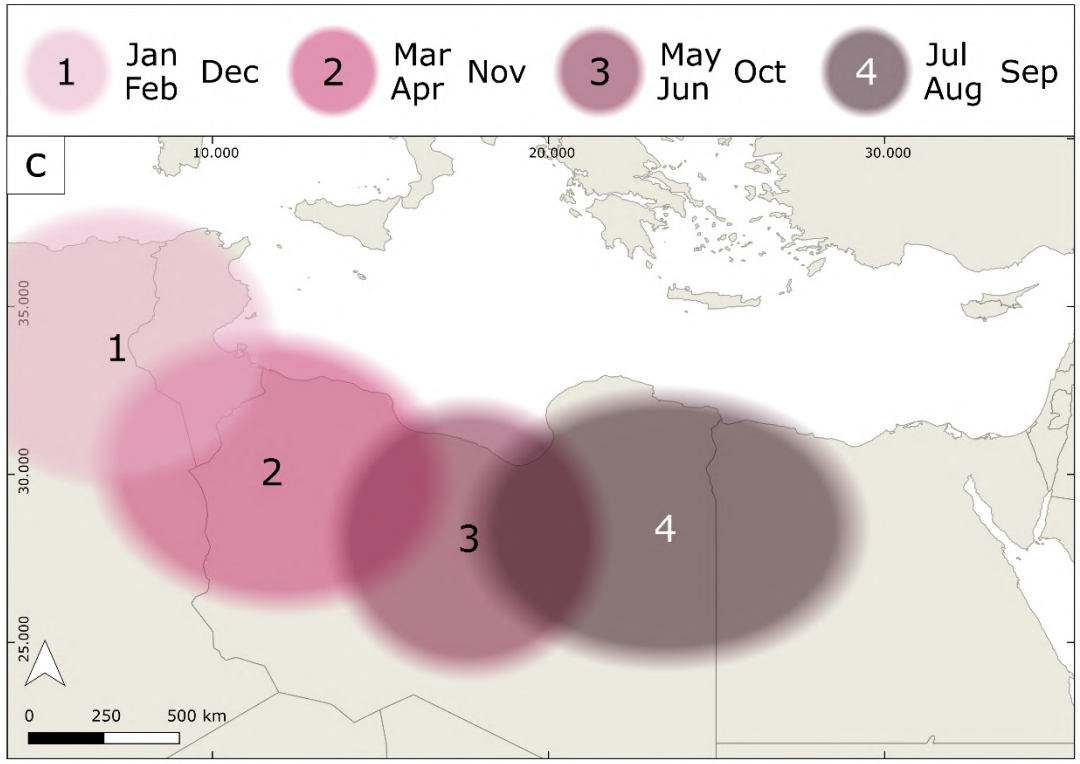


Figure 8: Schematic visualization of the dominance of primary long range mineral dust in deposition samples (Bitzan et al. unpublished data - under review)

Taking into account the spatial distribution of the minerals (particularly calcite and palygorskite) and the temporal distribution of their occurrence in the deposition samples, the following potential annual pattern of the dominant source regions emerges.

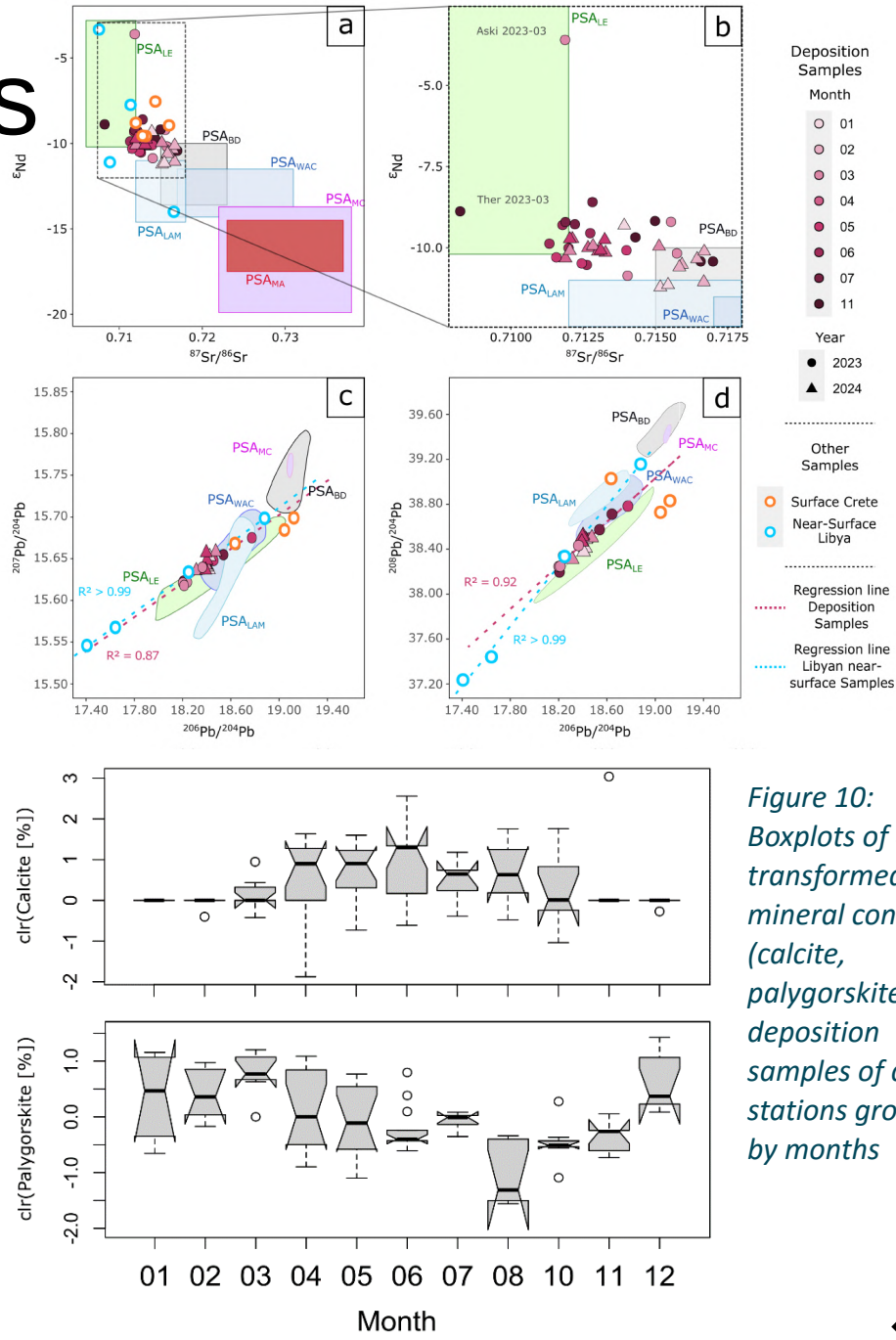


Figure 9: Isotopic ratios of Cretan deposition samples grouped according to sampling months (Sr, Nd, Pb)

Figure 10: Boxplots of clr-transformed mineral contents (calcite, palygorskite from deposition samples of all stations grouped by months

1.7 Main Findings from Fingerprinting

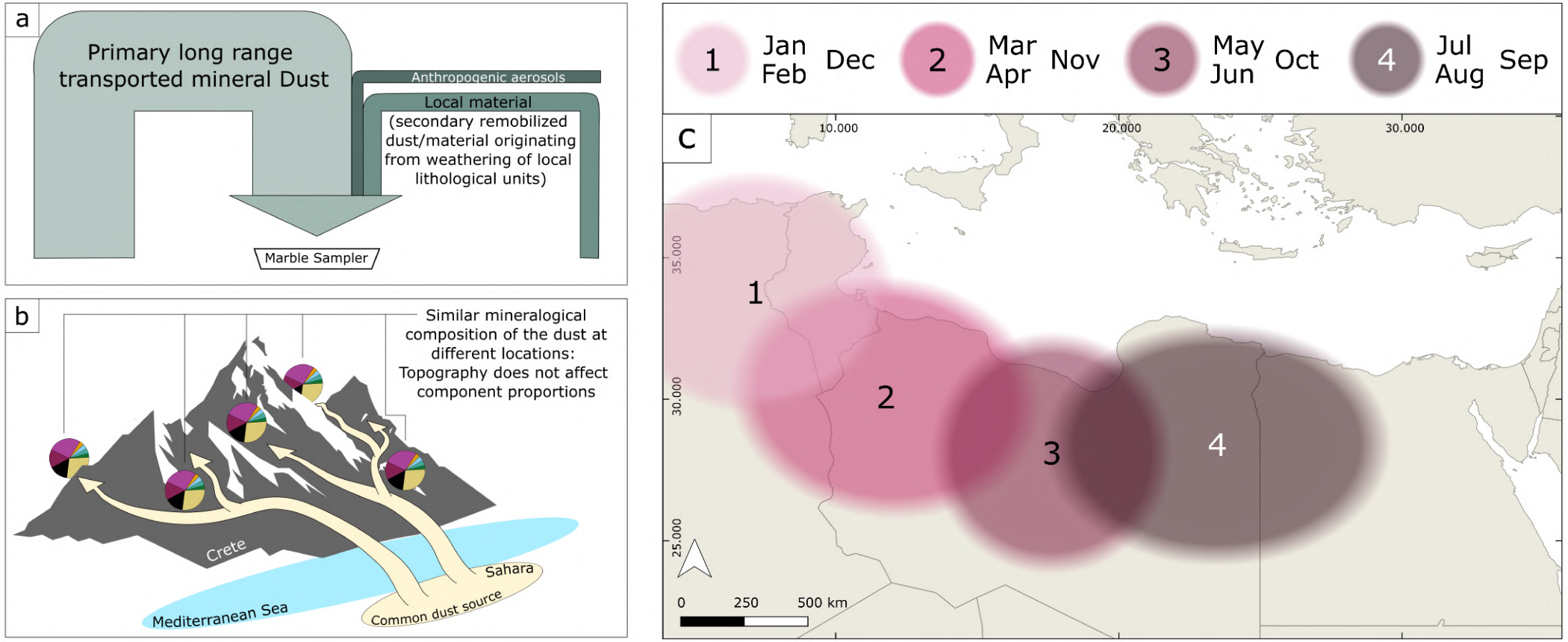
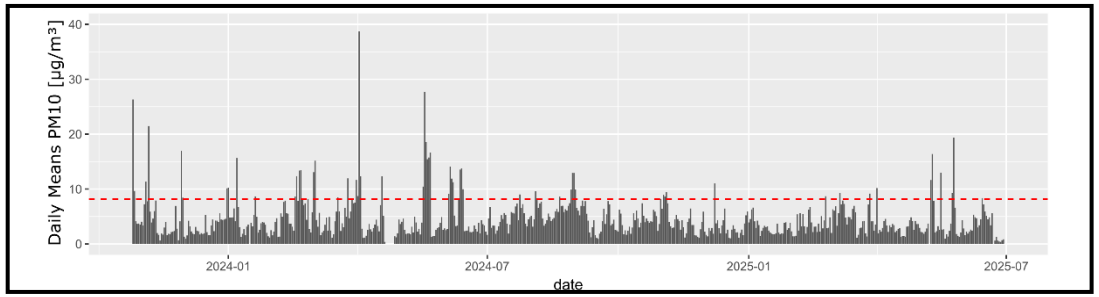


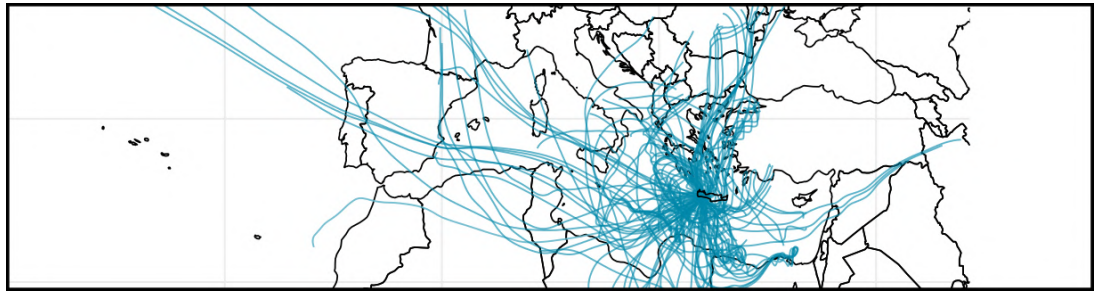
Figure 10: Schematic visualization of the main conclusions of the study: a – dominance of primary long range mineral dust in deposition samples; b – no detectable impact of topographic influences on mineralogical dust composition; c – dominant dust source areas over the course of the year regarding dust deposition on Crete (Bitzan et al. unpublished data - under review)

2. Trajectory Analyses

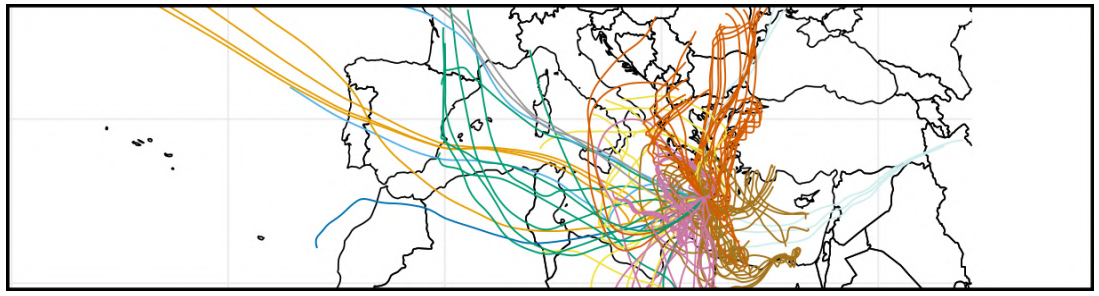
Definition of dust days by threshold



Calculate trajectories with HYSPLIT-model



Cluster analysis to identify spatial patterns connected to seasonal shifts



In Section 2, for the definition of dust days, the measurements of the optical particle sampler were used.

Backward trajectories were calculated at ground level for arrival times at 0, 6, 12, and 18 hours, based on the NCEP/ NCAR dataset.

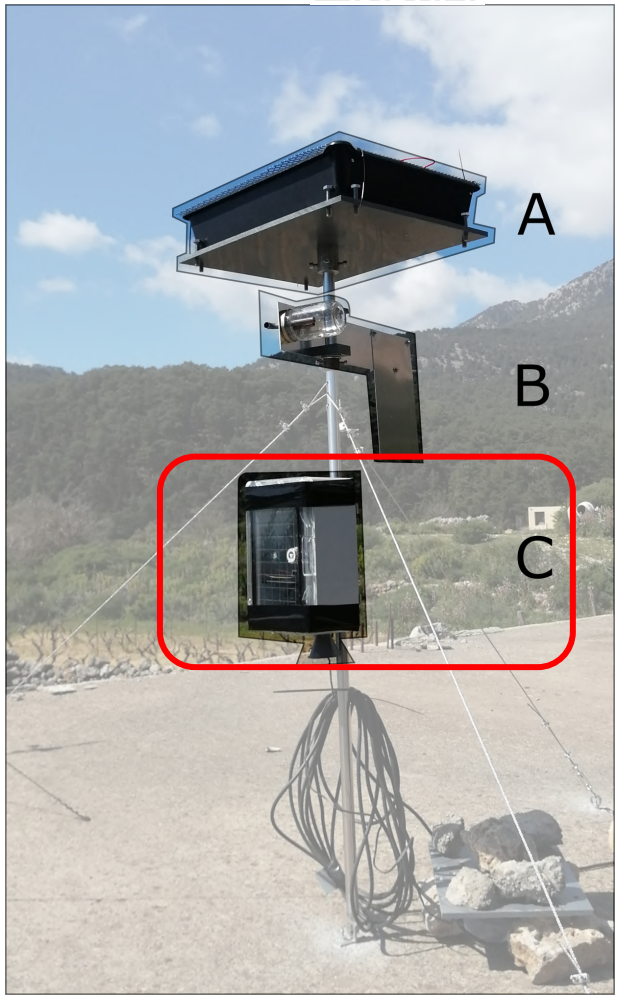


Figure 2: Sampling station in Agios Ioannis Sfakion. A - Marble Sampler; B - MWAC; C - OPC

2.1 Definition of Dust Days

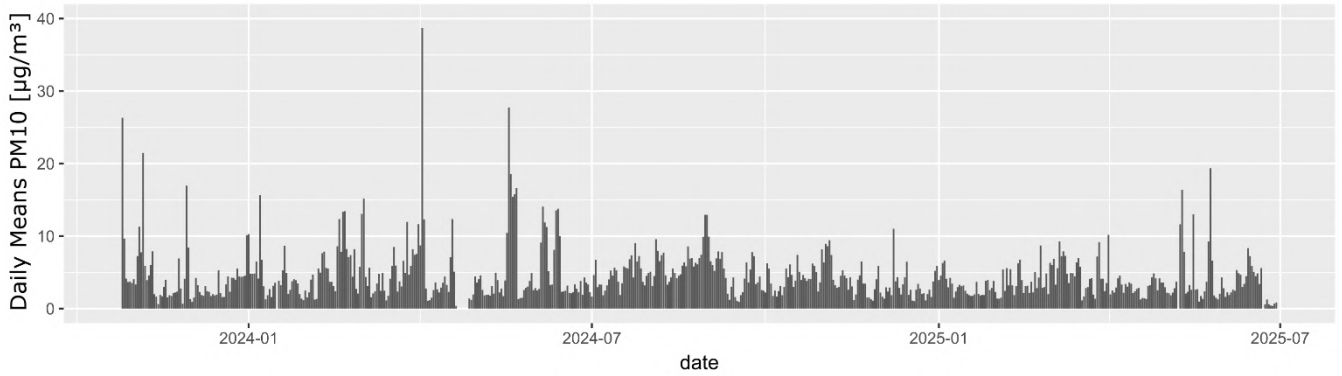


Figure 11: Daily means of aerosol concentration in Agios Ioannis, measured by optical particle counters

Dust days were defined as days on which daily mean concentrations exceeding 8.16 µg/m³ (85th percentile) were measured at at least three locations.

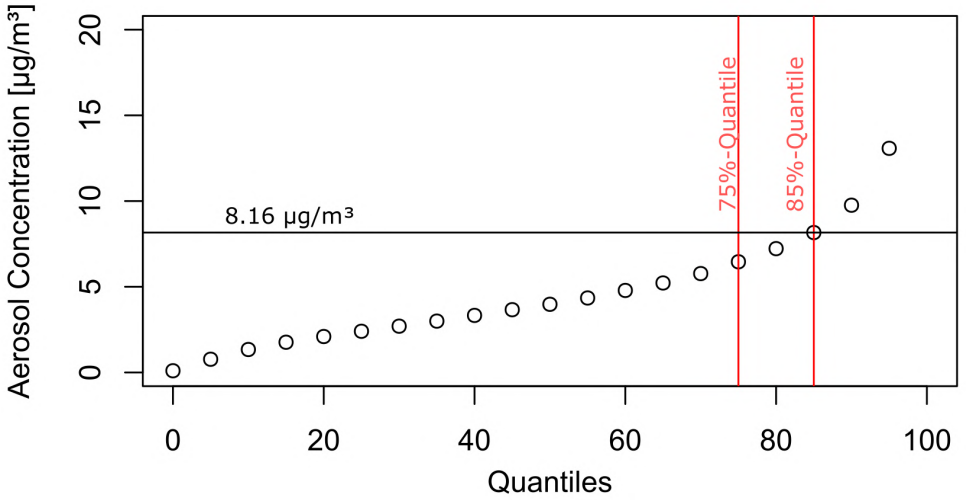


Figure 12: Quantiles of daily means of aerosol concentrations from all stations in 5%-steps

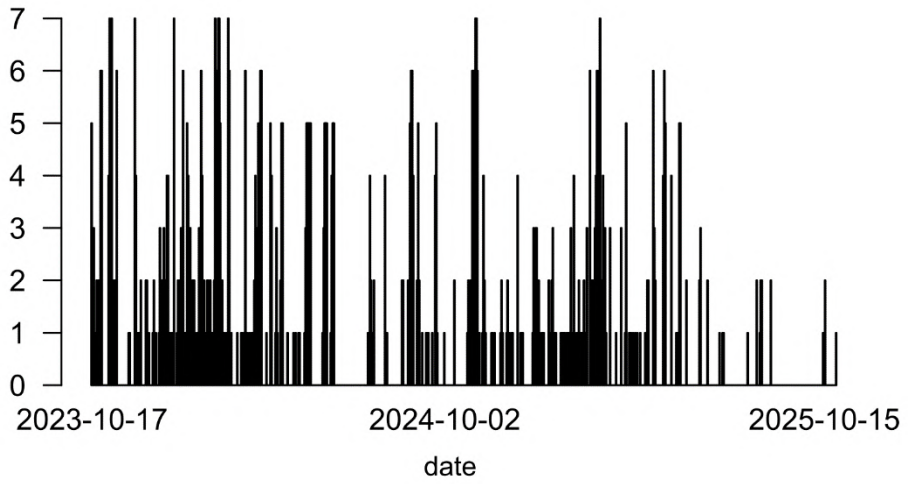
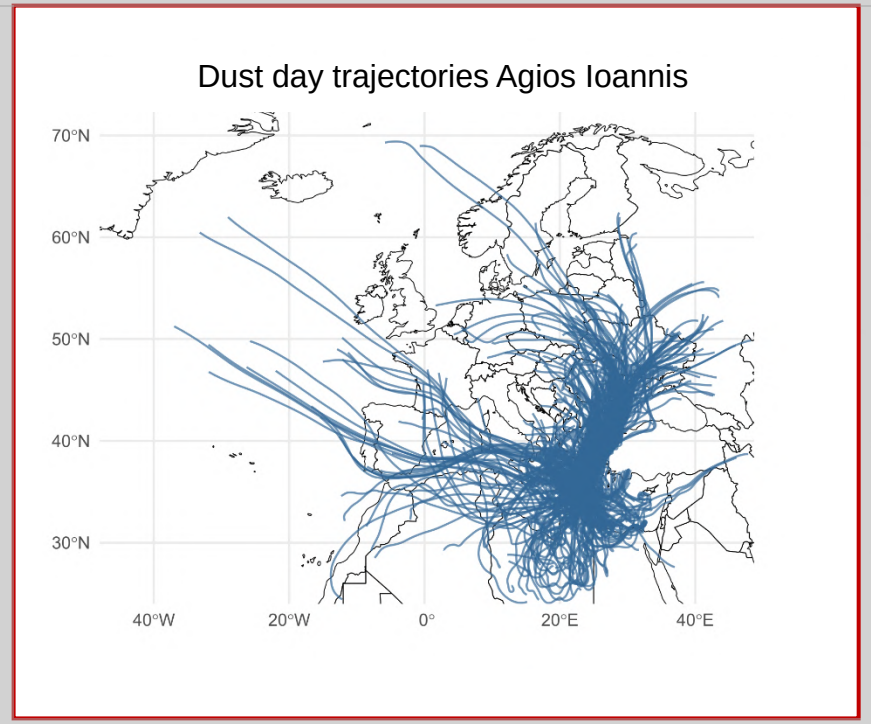
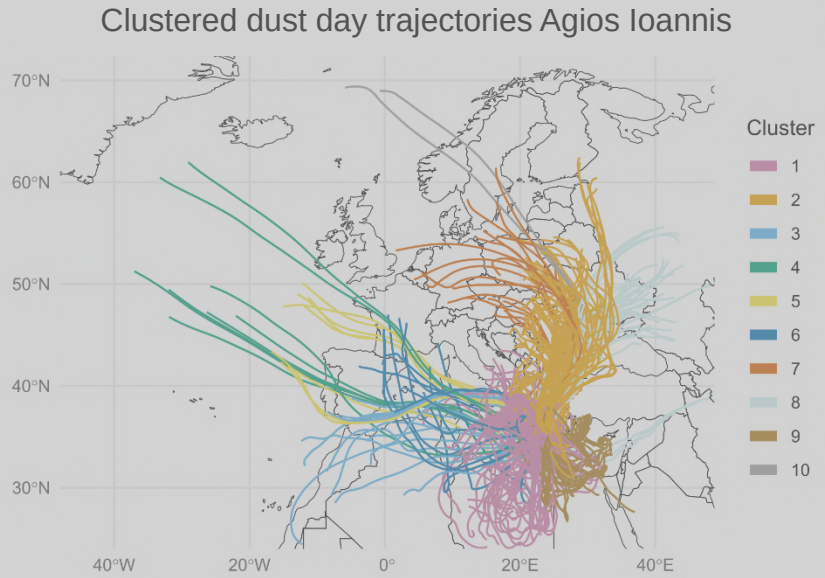


Figure 13: Number of stations that detected a dust day for each day between 10-2023 and 10-2025. According table on the right

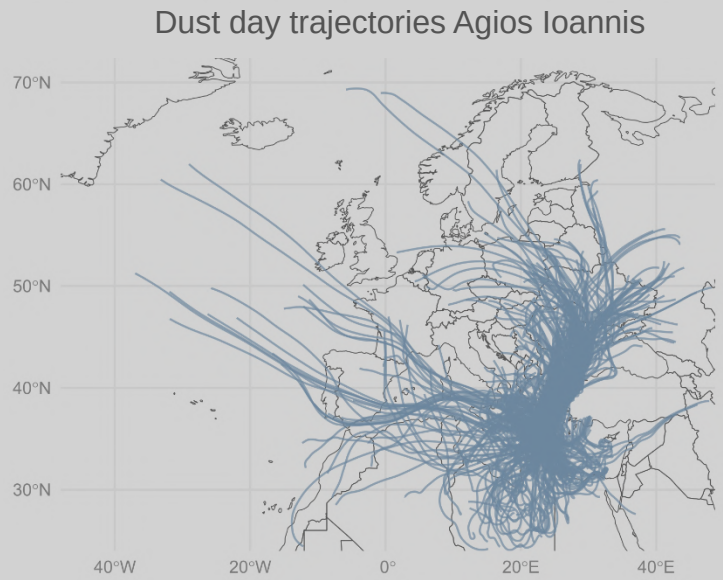
Number of stations	Number of days
0	432
1	142
2	64
3	25
4	23
5	24
6	21
7	11

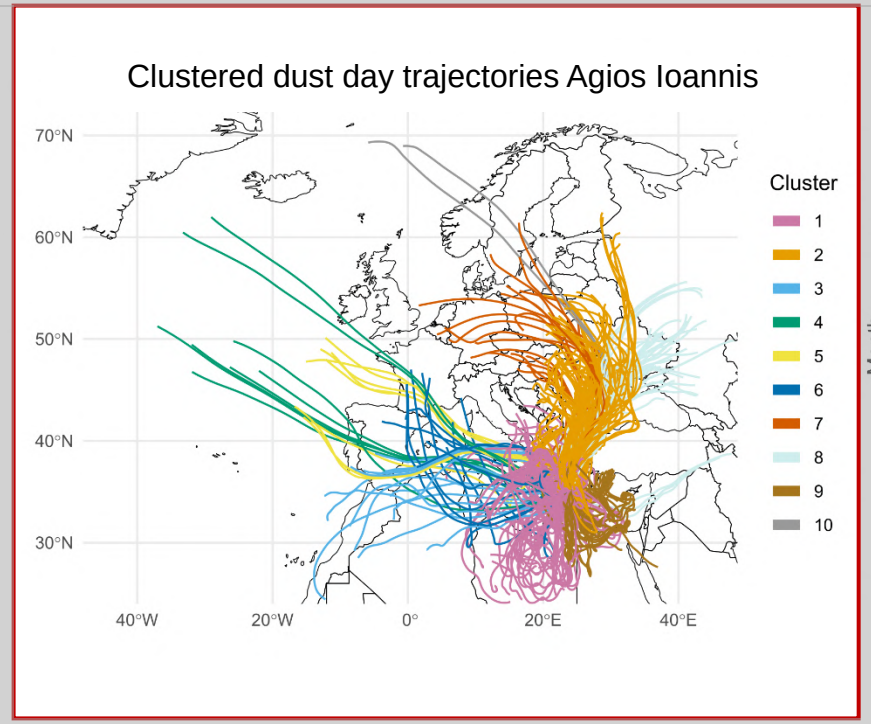
2.2 Trajectories and Cluster Analysis

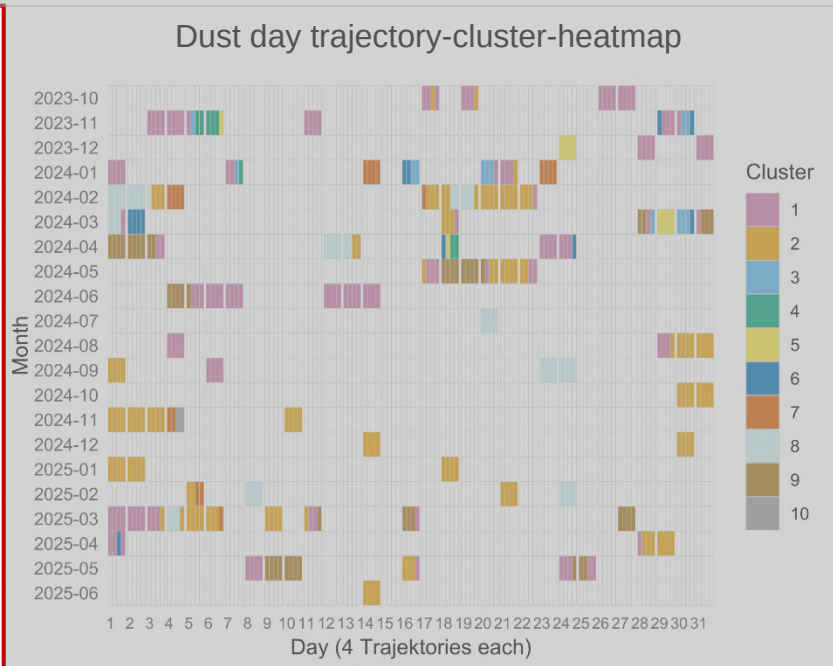




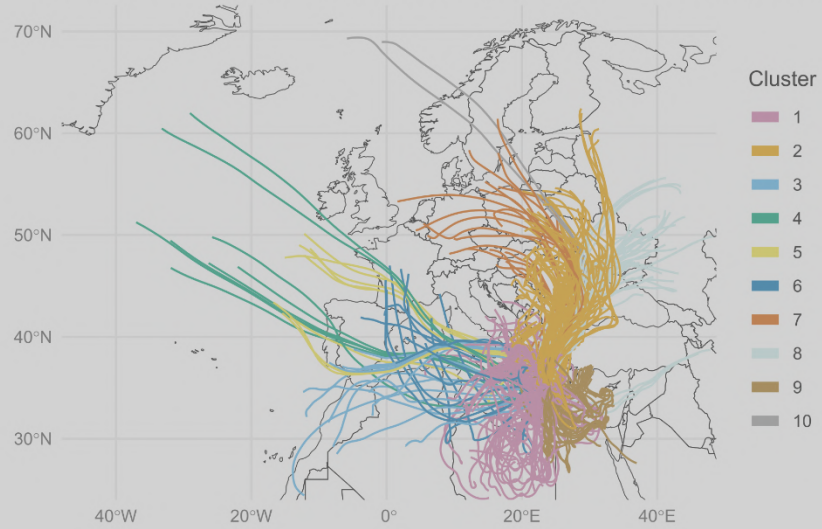
2.2 Trajectories and Cluster Analysis

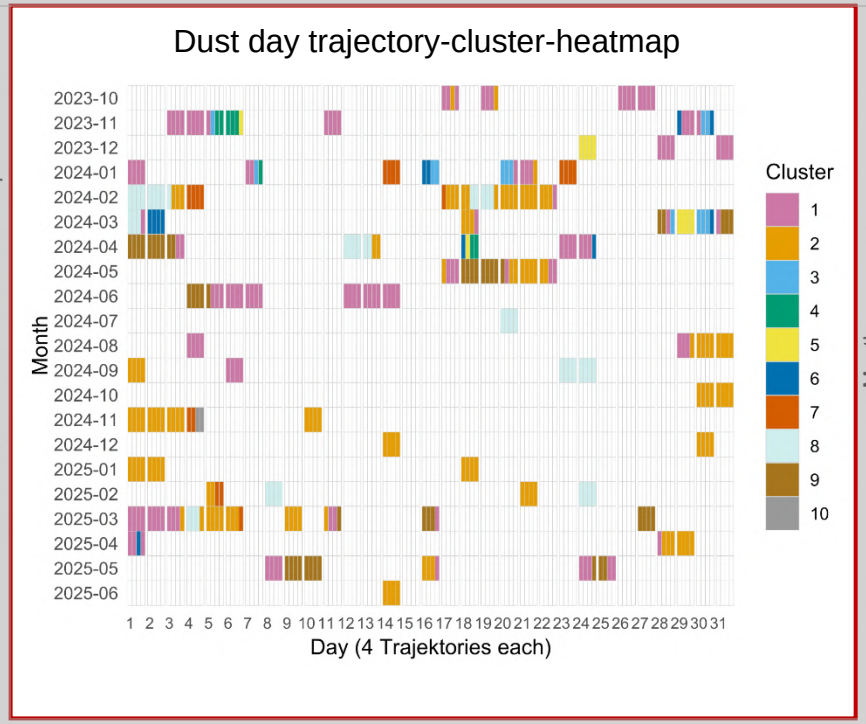


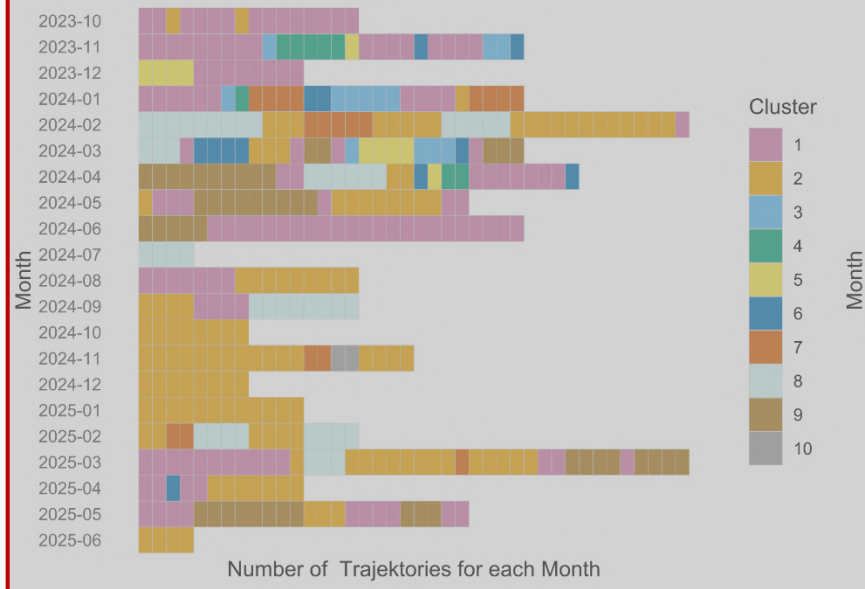




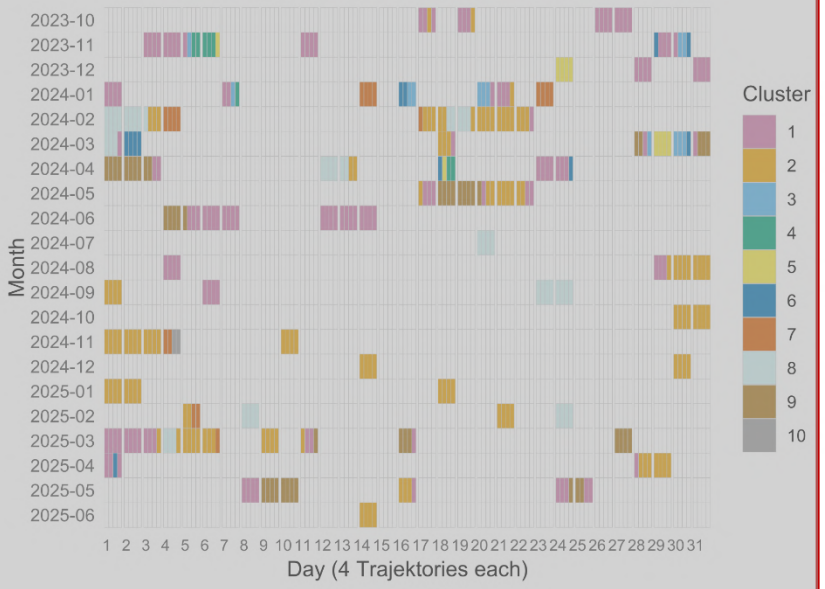
2.2 Trajectories and Cluster Analysis

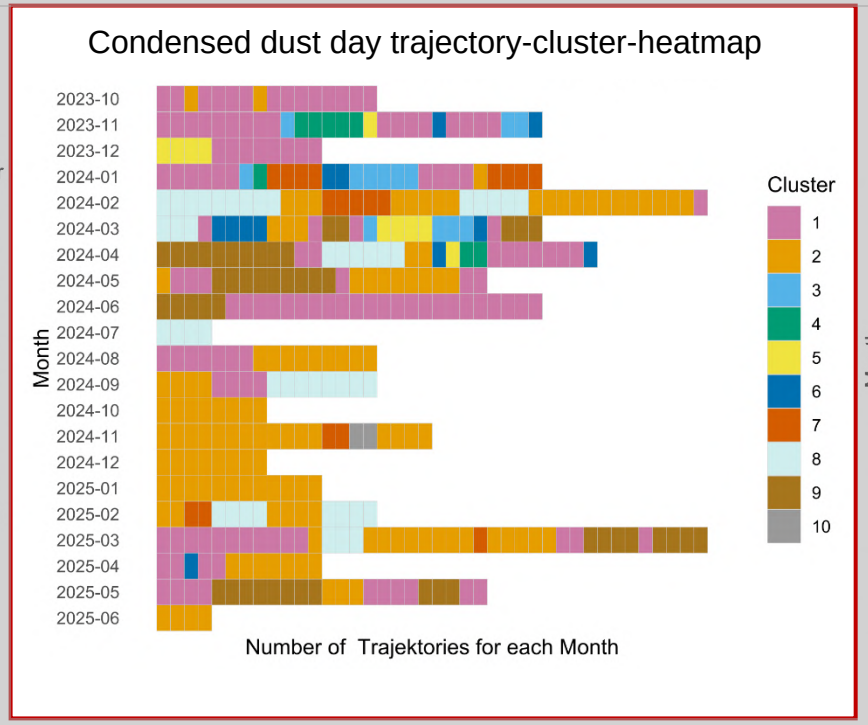


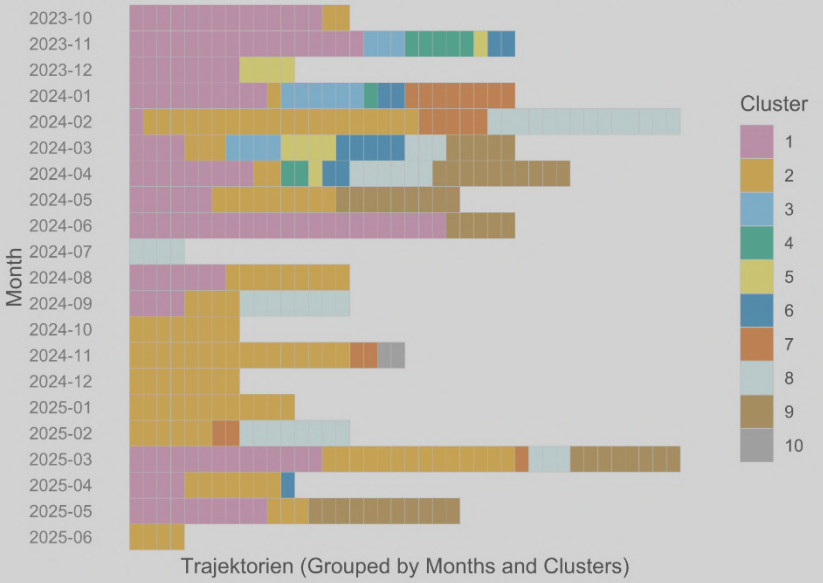




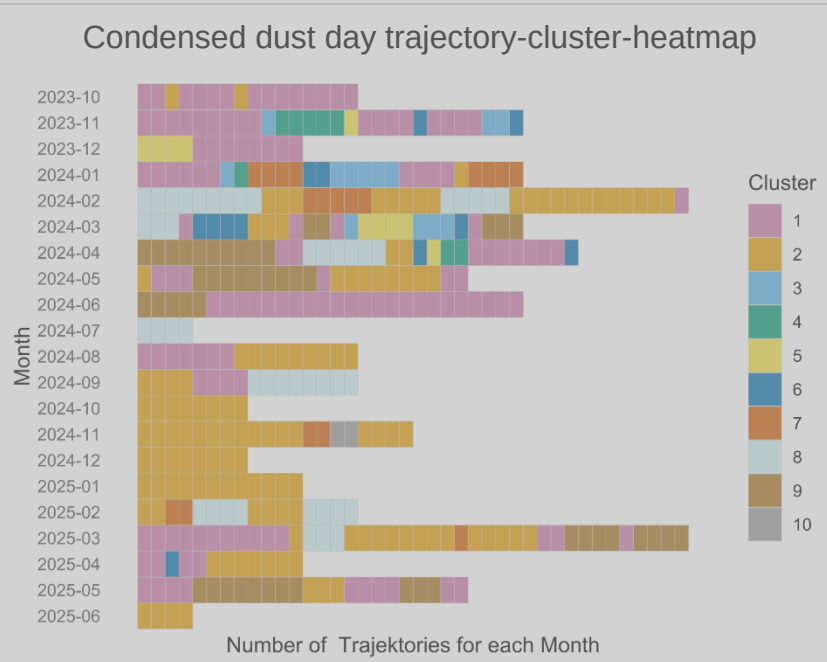
2.2 Trajectories and Cluster Analysis

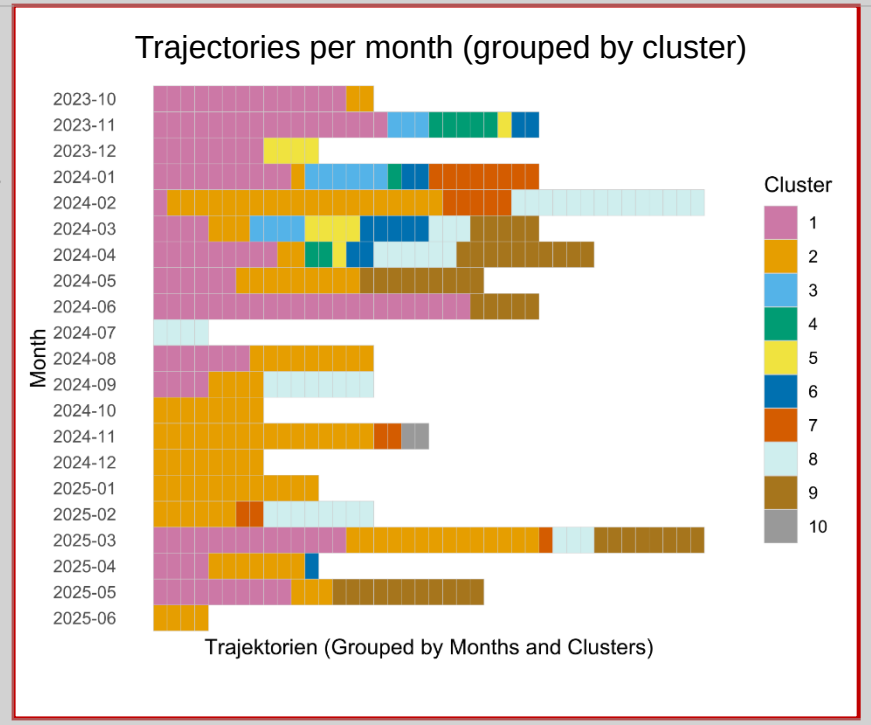






2.2 Trajectories and Cluster Analysis





2.2 Trajectories and Cluster Analysis

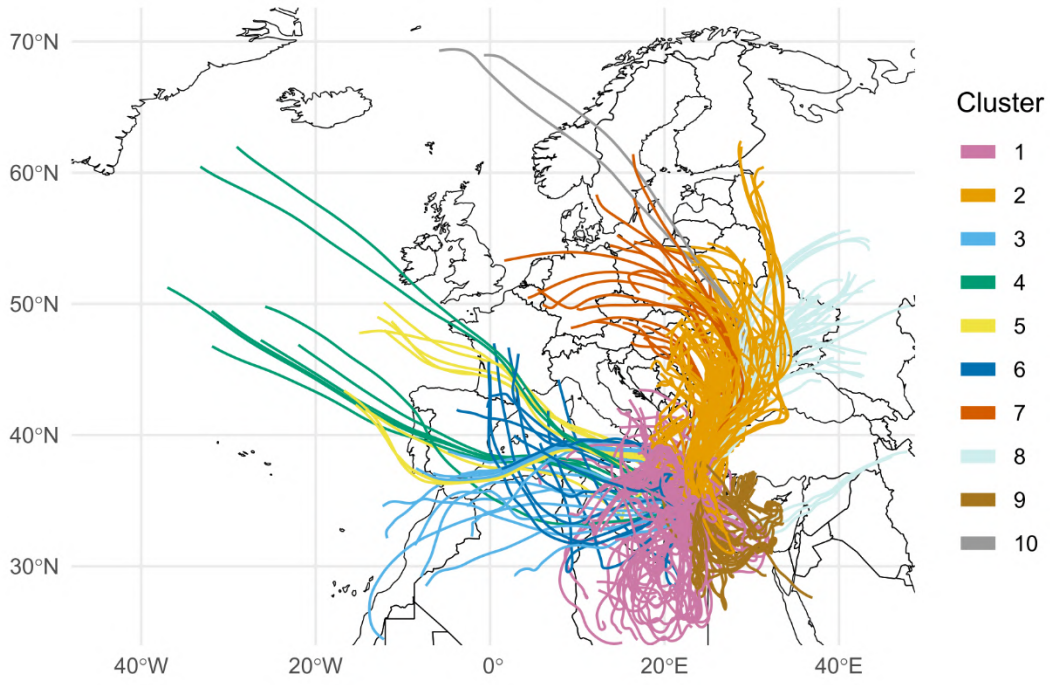


Figure 14: Clustered trajectories of all days on which at least three locations had daily means above the limit value (4 trajectories per day)

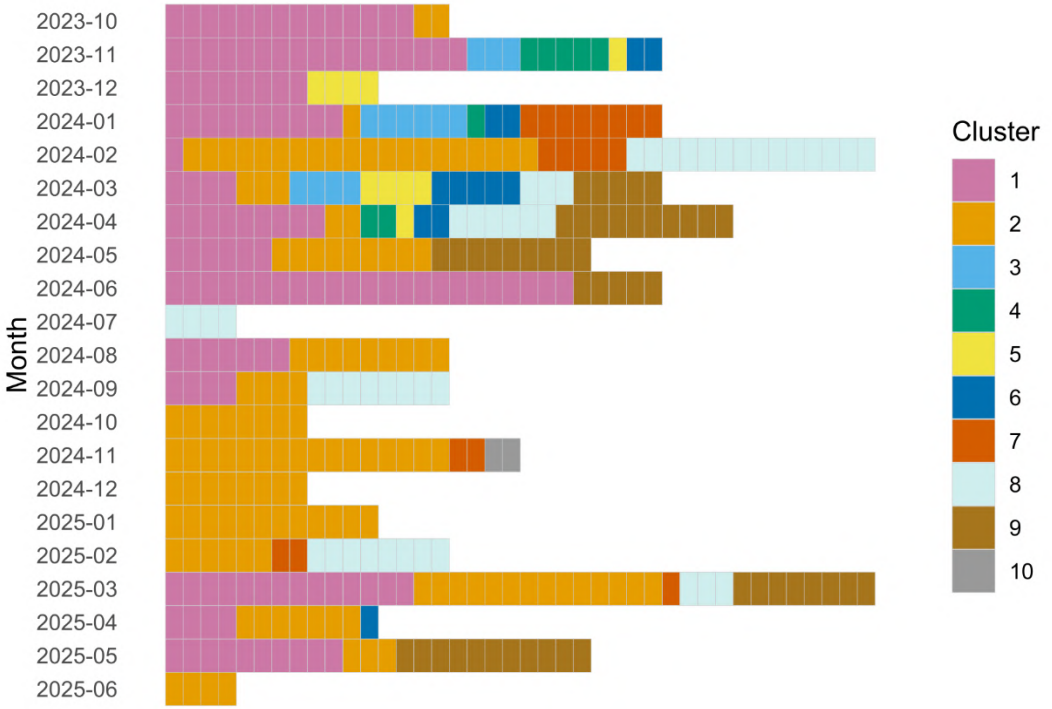


Figure 15: Cluster affiliations of all trajectories shown in the left figure. Grouped by months and affiliation

2.2 Trajectories and Cluster Analysis

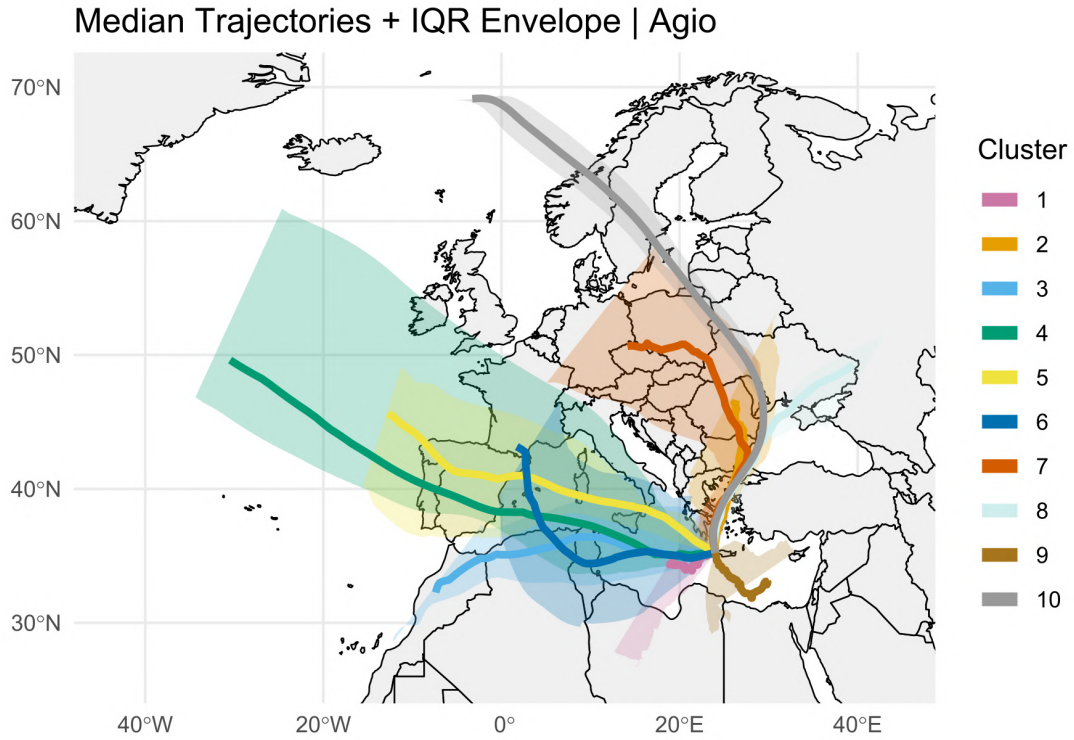


Figure 16: Cluster-wise median trajectories of all days on which at least three locations had daily means above the limit value. Hull equals Q10-Q90

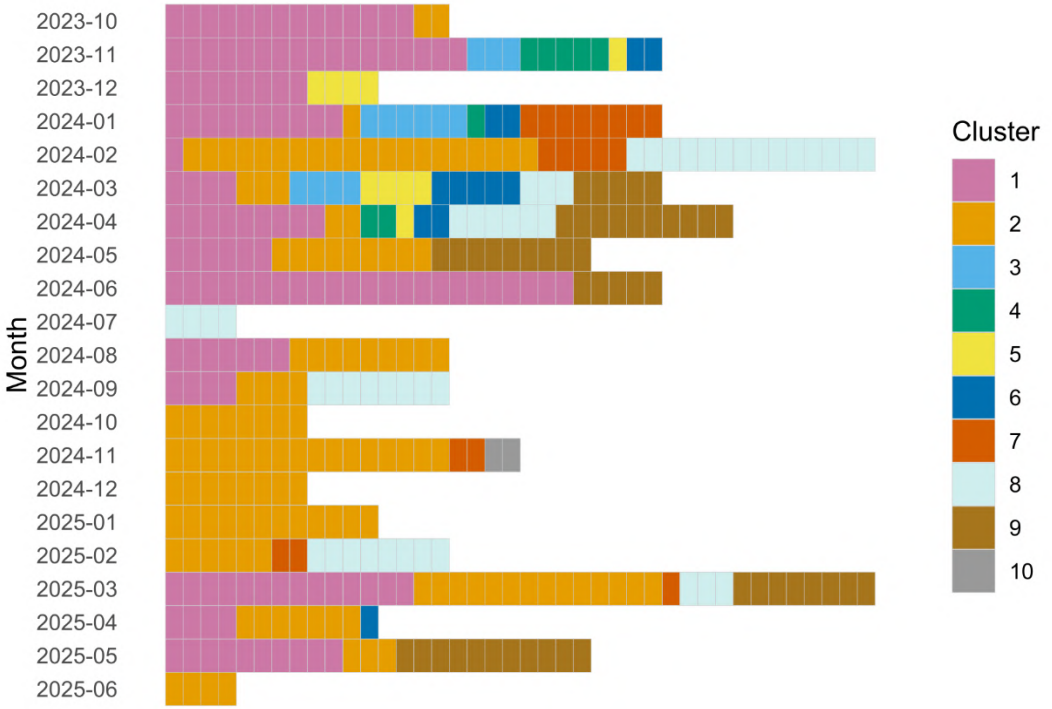


Figure 15: Cluster affiliations of all trajectories shown in the left figure. Grouped by months and affiliation

2.3 Regression Analysis

Only cluster 1, 2, 8, and 9 show significant differences on monthly occurences

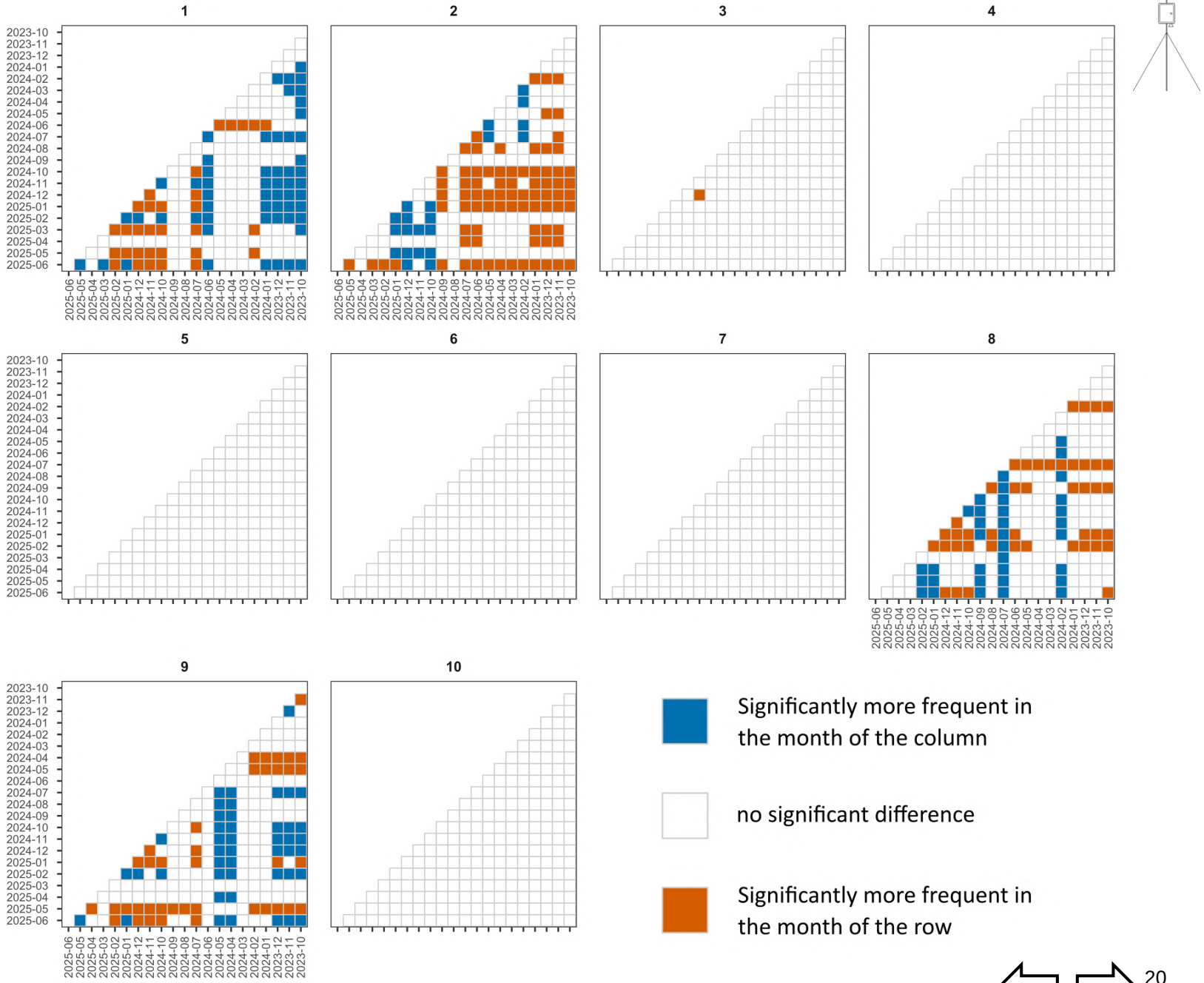


Figure 17: Significant differences in occurences of cluster affiliations over observation period (alpha = 0.5)

2.4 Compo-site-Plots

Cluster 1 and 9 show weaker pressure anomaly gradients than cluster 2 and 8

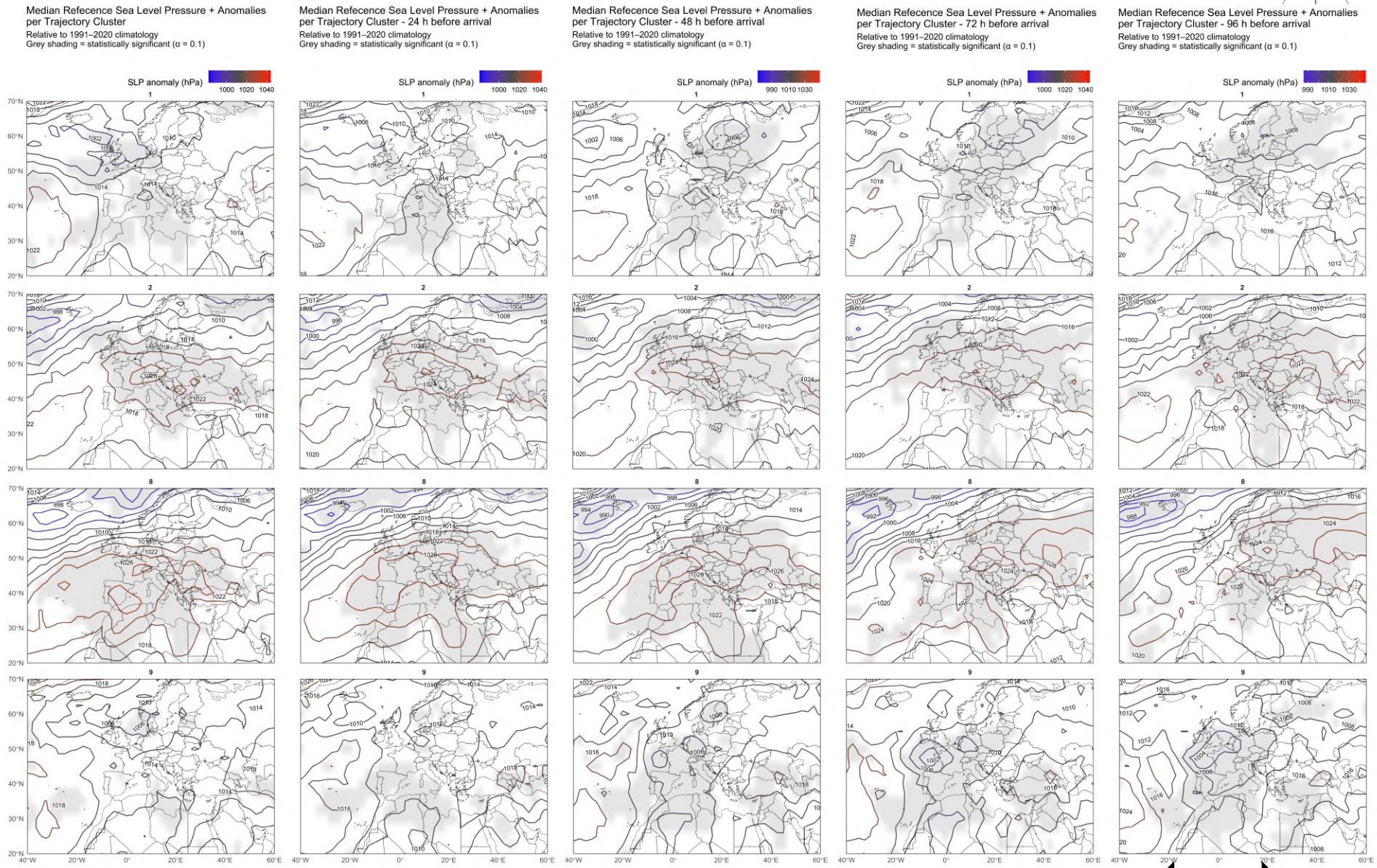


Figure 18: Composite plot of the sum of air surface level pressure anomalies between the days of the trajectories affiliated with the different clusters (1, 2, 8, 9) and a 30-year median climatology, and the 30-year median climatology

3. Conclusion

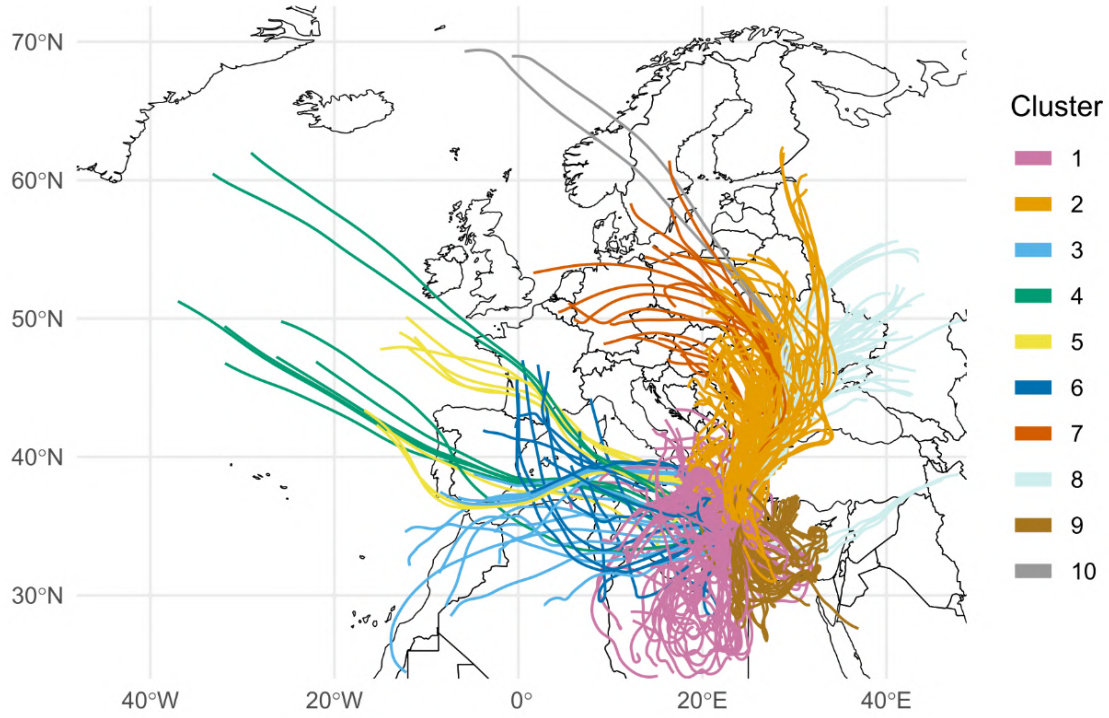


Figure 14: Clustered trajectories of all days on which at least three locations had daily means above the limit value (4 trajectories per day)

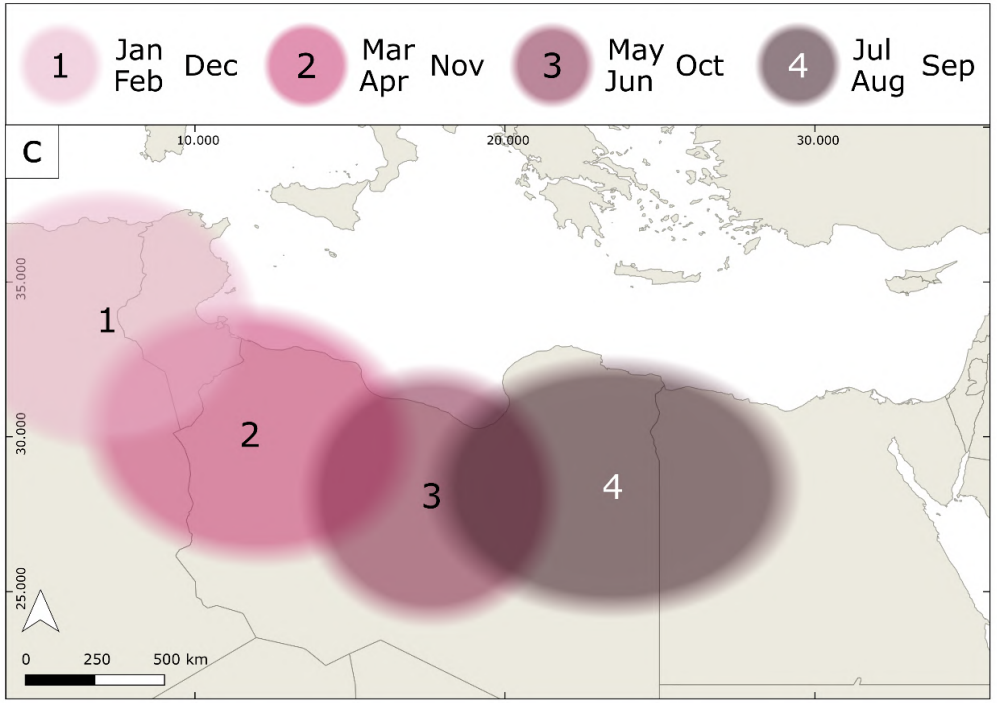


Figure 8: Schematic visualization of the dominance of primary long range mineral dust in deposition samples

- Clusters 1, 2, 8, and 9 are the clusters that occur more frequently at certain times of the year due to seasonality
- Clusters 1 and 9 reflect the typical transport pathways during their respective periods of occurrence, while clusters 2 and 8 result from pressure anomalies during those same periods
- It can therefore be assumed that clusters 1 and 9 are responsible for the majority of material transport to Crete.
- This is generally consistent with the findings of the provenance analysis based on the deposition samples.